

Inelastic neutron scattering study of the anisotropic $S = 1$ spin chain $[\text{Ni}(\text{HF}_2)(3\text{-Clpyridine})_4]\text{BF}_4$

 Daniel M. Pajerowski ^{1,*}, Jamie L. Manson ², Jacek Herbrych ^{3,4,5}, Jesper Bendix,⁶ Andrey A. Podlesnyak ¹,
 John M. Cain ⁷ and Mark W. Meisel ⁸
¹Neutron Scattering Division, Oak Ridge National Laboratory, Oak Ridge, Tennessee 37831, USA

²Department of Chemistry and Biochemistry, Eastern Washington University, Cheney, Washington 99004, USA

³Department of Theoretical Physics, Wrocław University of Science and Technology, 50-370 Wrocław, Poland

⁴Department of Physics and Astronomy, University of Tennessee, Knoxville, Tennessee 37996, USA

⁵Materials Science and Technology Division, Oak Ridge National Laboratory, Oak Ridge, Tennessee 37831, USA

⁶Department of Chemistry, University of Copenhagen, Universitetsparken 5, 2100 Copenhagen, Denmark

⁷Department of Chemistry, University of Florida, Gainesville, Florida 32611-8440, USA

⁸Department of Physics and the National High Magnetic Field Laboratory, University of Florida, Gainesville, Florida 32611-8440, USA


(Received 22 January 2020; accepted 7 March 2020; published 27 March 2020)

$[\text{Ni}(\text{HF}_2)(3\text{-Clpyridine})_4]\text{BF}_4$ (NBCT) is a one-dimensional, $S = 1$ spin chain material that shows no magnetic neutron Bragg peaks down to temperatures of 0.1 K. Previous work identified NBCT as being in the Haldane phase and near a quantum phase transition as a function of D/J to the large- D quantum paramagnet phase (QPM), where D is the axial single-ion anisotropy and J is the intrachain superexchange. Herein, inelastic neutron scattering results are presented on partially deuterated, ^{11}B -enriched NBCT polycrystalline samples in zero magnetic field and down to temperatures of 0.3 K. Comparison to density matrix renormalization group calculations yields $D/J = 1.51$ and a significant rhombic single-ion anisotropy E ($E/D \approx 0.03$, $E/J \approx 0.05$). These D , J , and E values place NBCT in the large- D QPM phase but precipitously near a quantum phase transition to a long-range ordered phase.

 DOI: [10.1103/PhysRevB.101.094431](https://doi.org/10.1103/PhysRevB.101.094431)
I. INTRODUCTION

Spin chains have played a foundational role in understanding many-body physics in the quantum regime, dating to nearly a century ago, and continue to yield interesting physics. Lower spin values naturally possess more quantum features, and the $S = 1/2$ and $S = 1$ isotropic chains have distinct ground states [1]. The $S = 1/2$ class of materials is unique in that it may be considered analytically via Bethe's approach, giving a gapless ground state [2]. Conversely, the isotropic $S = 1$ antiferromagnetic (AFM) spin chains do not have analytical solutions and have a nondegenerate gapped ground state that is called the Haldane phase [3–5]. These spin chains are also notable as prototypes for considering topologically ordered physics [6], having a hidden nonlocal order parameter [7].

The present work focuses on the effects of single-ion anisotropy on the ground state and excitations of $S = 1$ chains that may be characterized by the spin Hamiltonian

$$\begin{aligned}
 H = & J \sum_i \mathbf{S}_i \cdot \mathbf{S}_{i+1} + J' \sum_{(i,j)} \mathbf{S}_i \cdot \mathbf{S}_j \\
 & + D \sum_i (S_i^z)^2 + E \sum_i [(S_i^x)^2 - (S_i^y)^2], \quad (1)
 \end{aligned}$$

where $\mathbf{S}_i = (S_i^x, S_i^y, S_i^z)$, $J > 0$ is the AFM intrachain superexchange energy, J' is the interchain superexchange energy, the

$\langle i, j \rangle$ summation is between neighboring chains, D is the single-ion axial anisotropy, and E is the single-ion rhombic anisotropy. Theoretical consideration and numerical studies of Eq. (1) give rise to a complex phase diagram in J , J' , D , and E with an array of quantum critical boundaries and quantum multicritical points [8–11]. An additional term of exchange anisotropy has also been considered in the so-called XXZ chains [8,9]. Only more recently has the rhombic anisotropy been considered, and like D , it destabilizes the Haldane phase [10]. For $J' = 0$ and $E = 0$ without exchange anisotropy, the Haldane phase is bounded by the critical easy-plane anisotropy $D_C/J = 0.96845$ [8] and the critical easy-axis anisotropy $D_C/J = -0.32$ [9,11].

From the perspective of the dynamical (energy-resolved) correlation functions, spin chains described by Eq. (1) have a singlet ground state with propagating magnetic modes as excited states. For the isotropic case ($D = E = 0$) there is one mode of spin-spin correlations $\langle S^\alpha S^\alpha \rangle$ (with $\alpha = x, y, z$) that has a gap at the AFM zone center (often called the π point) of $\Delta = 0.41J$ [12]. Introducing D splits the propagating modes into longitudinal $\langle S^z S^z \rangle$ and transverse $\langle S^x S^x \rangle = \langle S^y S^y \rangle$ components. Finally, finite E splits the transverse mode, $\langle S^x S^x \rangle \neq \langle S^y S^y \rangle$.

Experimentally, compounds having various values of J , J' , D , and E have been reported. A summary of experimentally realized $S = 1$ spin chains for different J , J' , and D is given in Table 1 of Ref. [13], although E is not included there. It stands out that there is a large number of compounds that are well within the Haldane phase with $D/J < 0.25$ and compounds with $D/J > 4$ that are in the

*pajerowskidm@ornl.gov

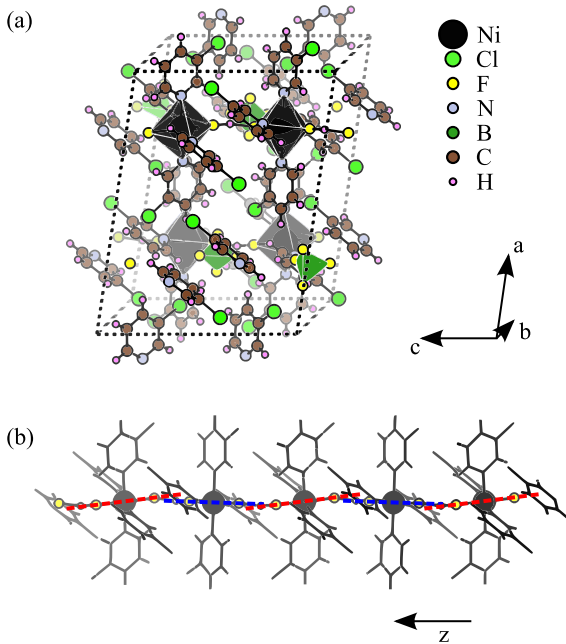


FIG. 1. NBCT crystal structure and chain motif. (a) The NBCT unit cell; NiF_2N_4 (black) and BF_4 (green) polyhedrons are shown. (b) A chain portion along the crystallographic c axis and the z axis of Eq. (1), with atoms not linking the chain suppressed. The dashed lines illustrate the relative canting between the two NiF_2N_4 moieties along the z (c) axis.

large- D quantum paramagnet (QPM) phase. It is exceptional that $[\text{Ni}(\text{HF}_2)(3\text{-Clpyridine})_4]\text{BF}_4$ (NBCT) is projected to have $D/J \approx D_C/J \approx 1$.

The NBCT system is a coordination polymer with $S = 1$ Ni^{2+} magnetic ions octahedrally coordinated as NiF_2N_4 , where the nickel chains are separated by large chloropyrazine ligands and the intrachain nickel bonds are via Ni-F-H-F-Ni linkages [Fig. 1(a)] [14]. The physical chain separation of >10 Å without any apparent electron hopping pathways makes a strong case for $J' \approx 0$ in NBCT. There is a 34° canting angle between the unique axes of the nickel along the chain [Fig. 1(b)]. The unit cell parameter along the chain c axis is 12.291 Å, and there are two nickel ions within the unit cell along this direction such that the π point is at a momentum of 0.511 \AA^{-1} . The initial identification of $D/J = 0.88$ for NBCT was derived by fitting the high-temperature susceptibility, assuming $D = 0$, to obtain $J = 4.86 \text{ K}$ (0.42 meV) and $g = 2.10$ and UV-visible data to extract $D = 4.3 \text{ K}$ (0.37 meV). No E value has been reported. The proximity of NBCT to a phase boundary was also inferred from isothermal magnetization studies that used randomly arranged microcrystals cooled down to 50 mK and an upper limit for a possible critical magnetic field (which could indicate the existence of the gap) was given as $H_C \lesssim 35 \pm 10 \text{ mT}$ [15].

Here, to further characterize the NBCT material, we have used inelastic neutron scattering (INS) experiments and density matrix renormalization group (DMRG) [16] calculations. The INS technique can directly probe time and space spin correlations in materials and has therefore been extensively used to investigate spin chain materials [17]. In the following,

we use INS from isotopically enriched powder samples to quantify the collective magnetic modes in NBCT at $T = 0.3 \text{ K}$. The observed spectra are then compared with $T = 0$ DMRG calculations of the dynamical spin structure factor $S(q, \omega)$ of Eq. (1) with $J' = 0$ to extract D , J , and E . The important findings are that $D/J = 1.51$ and $E/J \approx 0.05$ for our isotopically doped sample of NBCT. These results are in striking contrast to the $D/J = 0.88$ value reported for NBCT without isotope doping using bulk probes. The concluding section frames the present results in the context of the existing literature and provides suggestions for future studies of this unique system. Additional technical details are given in the Appendixes.

II. RESULTS AND DISCUSSION

Neutron spectra were collected at $T = 0.07 \text{ K}$ and showed no additional magnetic Bragg scattering (e.g., no magnetic ordering down to that temperature), but the background multiple scattering from that setup proved problematic for measuring inelastic features. Additional INS measurements were performed with a different cryostat at $T = 0.3$ and 13 K for incident energies E_i of 1.00, 1.55, 3.32, and 7.00 meV. No magnetic signal was observed above energy transfers of $\hbar\omega \approx 1.2 \text{ meV}$. The one-dimensional scattering function for NBCT was extracted from the powder data using the reported method [18]. For the $E_i = 3.32 \text{ meV}$ data, the dispersionless $T = 13 \text{ K}$ data were subtracted from the $T = 0.3 \text{ K}$ data to remove extrinsic multiple scattering signatures, while the $E_i = 1.00 \text{ meV}$ data have no such subtraction. A lattice-periodic dispersive mode is visible in the $E_i = 3.32 \text{ meV}$ data [Fig. 2(a)]. Two gaps at $q_{1D} = \pi$ ($Q_{1D} \approx 0.51^{-1}$) are visible in the $E_i = 1.00 \text{ meV}$ data [Fig. 2(c)], with values of $\Delta_1 = 0.057 \text{ meV}$ and $\Delta_2 = 0.111 \text{ meV}$ from the fits described below. The momentum transfer along the chain is Q_{1D} , and the unitless momentum q_{1D} varies from 0 to 2π in the Brillouin zone.

To extract Hamiltonian parameters, the experimental data were compared to DMRG calculations. For the $E_i = 3.32 \text{ meV}$ data, the optimization region is between $\hbar\omega = [0.8, 1.3] \text{ meV}$ and $Q_{1D} < 1^{-1}$. For the $E_i = 1.00 \text{ meV}$ data, the optimization region is between $\hbar\omega = [0.045, 0.400] \text{ meV}$ and $Q_{1D} = [0.44, 0.60]^{-1}$. Initial conditions for the fitting were $D/J = [0, 0.5, 1.0, 1.5, 2.0]$, with J values initialized to have the model zone boundary peak intensity at $\hbar\omega = 1.1 \text{ meV}$. These fits have three intrinsic parameters, D , J , and Δ_E , where Δ_E captures the effect of the rhombic E term by modifying that gap of the $\langle S^{x/y} S^{x/y} \rangle$ mode $\Delta_{x/y} \rightarrow \Delta_{x/y} \pm \Delta_E/2$ with $\Delta_{x/y} = (\Delta_1 + \Delta_2)/2 = 0.084 \text{ meV}$. There is one extrinsic parameter that scales the overall intensity. The relative intensity between $E_i = 3.32 \text{ meV}$ and $E_i = 1.00 \text{ meV}$ was taken from the known flux difference of those energies, the momentum resolution was taken from Bragg peaks, and the energy resolution used the semiempirical model that was developed for the spectrometer. The lowest residuals were found with the $D/J = 1.51$ parameters in Table I, which yield the spectra in Figs. 2(b) and 2(d).

A more quantitative visualization of the best-fit model compared to the data is possible by integrating over some momentum regions. The splitting of the gap at $q_{1D} = \pi$ and

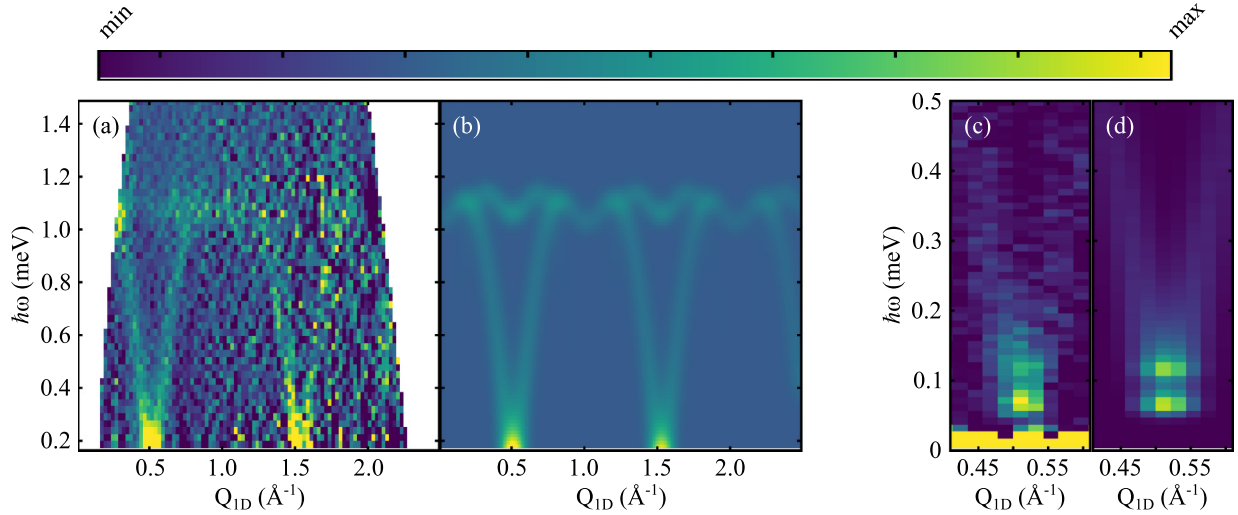


FIG. 2. Intensity maps of reverse-power-averaged NBCT experimental data and the DMRG model. (a) $E_i = 3.32$ meV, $T = 0.3$ K data minus $T = 13$ K data. White regions are where the scattering condition is not satisfied by the spectrometer. (b) $E_i = 3.32$ meV model that is calculated at $T = 0$ but includes a $T = 0.3$ K Bose factor correction. For (a) and (b) the intensity scale has $\text{min} = -2 \times 10^{-4}$ and $\text{max} = 5 \times 10^{-4}$ with scaled units. (c) $E_i = 1.00$ meV, $T = 0.3$ K data. (d) $E_i = 1.00$ meV that is calculated at $T = 0$ but includes a $T = 0.3$ K Bose factor correction. For (b) and (d) the intensity scale has $\text{min} = 0$ and $\text{max} = 2 \times 10^{-4}$ with scaled units.

quantitative gap-energy fitting of the model to the data are shown in Fig. 3. Some higher-energy lines further illustrate the good quantitative agreement of the $D/J = 1.51$ model with the INS data [Figs. 3(b)–3(d)]. This higher-energy spectral weight is essential to the model, as without it the gap energies have no context, and there is also information regarding the dispersivity of the $\langle S^z S^z \rangle$ mode. It is unclear if the incorrect model intensity in Fig. 3(a) shows an intrinsic effect or is merely due to a difference between the recorded thermometer temperature and the actual sample temperature (a temperature of $T \approx 0.6$ K would increase the model intensity of the lowest mode and reproduce the experimentally observed ratio of the two modes). Indeed, it may be that the difficulty in cooling is due to a large entropy contribution of the ground state.

When starting INS model optimization with the $D/J = 0.5$ initial condition, a local minimum exists with residuals $> 10\%$ larger than the best fit that is a similar distance in D/J from the critical D_C/J value and with parameters of $J = 0.41$ meV, $D = 0.18$ meV, $D/J = 0.44$, and $\Delta_E = 0.05$ meV. While fitting the gap well, the $D/J = 0.44$ fit is qualitatively different from the data as it has an $\langle S^z S^z \rangle$ mode with significant intensity at $(q_{1D}, \hbar\omega) = (\pi, 0.44$ meV) that would be greater than five times the observation and miss the intensity at the top of the band at the AFM zone boundary.

In addition to the one-dimensional collective modes, a local mode was observed at low temperatures (Appendix B). This local mode is not visible in the data converted from $|Q|$ to Q_{1D} because it does not have a one-dimensional momentum

dependence of the intensity. In the unconverted data, there is a momentum-independent (aside from the Ni^{2+} magnetic form factor) peak at 0.53 meV that is precisely the best-fit value of D . We assign this feature to be single-ion D excitations from Ni^{2+} spins that are in environments that have chain lengths less than the correlation length.

Our neutron data give different parameters from the ones that were derived from bulk measurements but have values that are close to being within the bulk parameter experimental uncertainties. The $D/J = 0.44$ solution has $D = 0.18$ meV, which is low for NiF_2N_4 [19]. Then with $D/J = 1.51$, NBCT is in the large- D QPM phase in (D, J) space.

To understand the position of NBCT in a spin chain phase diagram and look for possible quantum phase transitions, the magnitude of the rhombic single-ion anisotropy must be estimated. The $\text{Ni}(\text{C}_2\text{H}_8\text{N}_2)_2\text{NO}_2\text{ClO}_4$ (NENP) material with $D/J = 0.18$ was reported to have $E/D = 0.11$ [20]. A survey of large- D QPM phase chains shows a range of E/D values from 0.1 to 0.3 [21]. Wave function theory calculations of NBCT give $D = 13.44$ K (1.16 meV) and $E = 1.80$ K (0.155 meV) such that $E/D = 0.13$, while wave function theory calculations of a molecular analog of NBCT give $D = 7.12$ K (0.61 meV) and $E = 1.49$ K (0.128 meV) such that $E/D = 0.21$. Inputting the experimental gap values to the perturbation theory expansion of D and E [22] gives $E = 0.07$ meV and $E/D = 0.13$. Taking the experimental INS $J = 0.35$ meV for NBCT from Table I scales E/D values of 0.13 and 0.21 to E/J values of 0.20 and 0.31, respectively. These calculations clearly show the non-negligible character of E in NBCT and related compounds. Also, the relative canting of the local quantization axes for the two magnetic Ni^{2+} ions in the unit cell (Fig. 1) will have the effect of a rhombic single-ion anisotropy on the collective modes and has the potential to modify the local single-ion values. Presumably, the splitting of the $\langle S^{x/y} S^{x/y} \rangle$ mode as a function of E will eventually close the gap on the lowest mode, and

TABLE I. Best-fit parameters of NBCT. Uncertainties are from fitting to least squares.

	J (meV)	D (meV)	D/J	Δ_E (meV)
NBCT	0.35 ± 0.01	0.53 ± 0.01	1.51 ± 0.01	0.05 ± 0.01

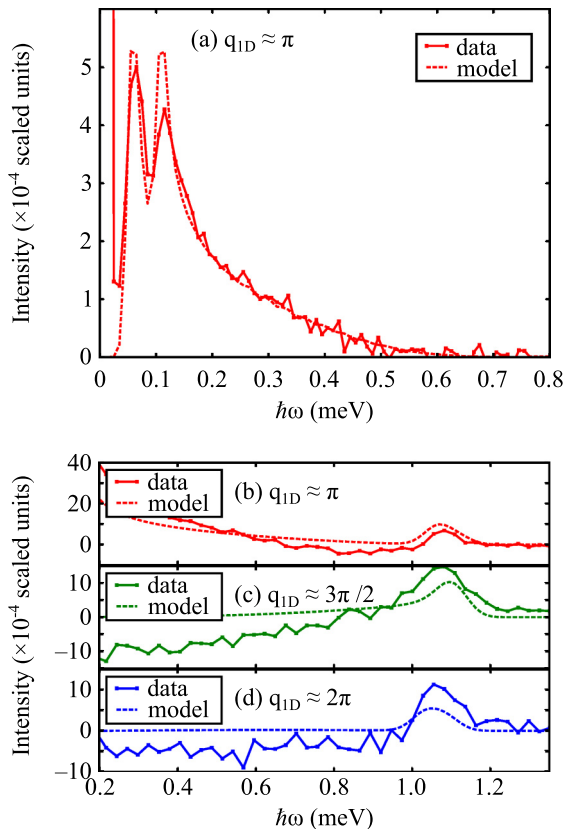


FIG. 3. Intensity versus energy transfer for reverse-power-averaged NBCT experimental data and the DMRG model. (a) Data and model of $E_i = 1.00$ meV, $T = 0.3$ K are shown for $Q_{1D} = [0.44, 0.57]^{-1}$. Data and model of $E_i = 3.32$ meV, $T = 0.3$ K are shown for (b) $Q_{1D} = [0.41, 0.65]^{-1}$ centered on the π point, (c) $Q_{1D} = [0.66, 0.90]^{-1}$ centered on the $3\pi/2$ point, and (d) $Q_{1D} = [0.91, 1.15]^{-1}$ centered on the 2π point. The negative intensities in $E_i = 3.32$ meV are most likely due to oversubtraction of the $T = 13$ K data that has quasielastic magnetic scattering.

long-range order will appear. If at $D/J = 1.51$ the critical E_C/J is estimated to be ≈ 0.11 , then a linear dependence of the energy splitting yields $E/J = 1.3 \Delta_E$ for NBCT and $E/J = 0.07$. We performed an additional DMRG calculation with $D/J = 1.51$ and $E/J = 0.07$, which yield (for $J = 0.35$ meV) $\Delta_1 = 0.046$ meV, $\Delta_2 = 0.129$ meV, and $\Delta_E = 0.083$ meV. The INS $\Delta_E = 0.054$ (0.05 ± 0.01) meV implies $E/J < 0.07$ for NBCT, and then $E/J \approx 0.05$ ($E/D \approx 0.03$), assuming that $\Delta_E \propto E/J$ near $E/J = 0.07$. Indeed, the absence of magnetic Bragg scattering at temperatures significantly less than the exchange energy scale is in opposition to a magnetically ordered ground state for NBCT, while the low-temperature specific heat [14] and magnetization data [15] may indicate the nearby presence of strong quantum fluctuations. Finally, NBCT may be plotted on the $(D/J, E/J)$ phase diagram [10] (Fig. 4) and is close to the predicted boundary between a large- D phase and a magnetically ordered phase.

III. CONCLUSIONS AND OPEN QUESTIONS

The magnetic excitations in isotopically enriched $[\text{Ni}(\text{HF}_2)(3\text{-Clpyridine})_4]\text{BF}_4$ (NCBT) were measured at

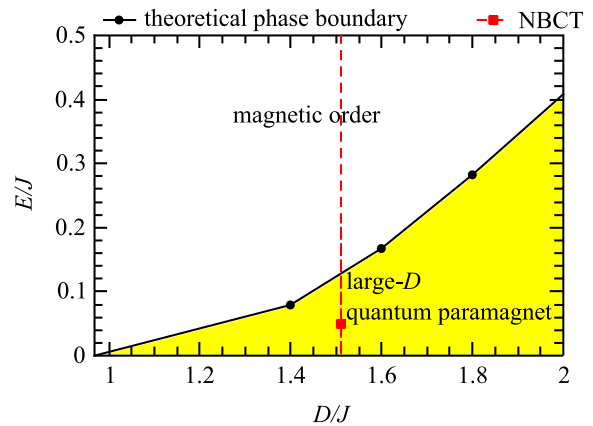


FIG. 4. Anisotropic spin chain phase diagram. The theoretical phase boundary is from Ref. [10]. The $D/J = 1.51$ line is shown along with a marker for $E/J = 0.05$, which places NBCT in the large- D QPM phase but close to a long-range ordering transition.

$T = 0.3$ K using inelastic neutron scattering techniques on a sample of randomly arranged microcrystals. These data were combined with numerical density-matrix renormalization group studies to find $D/J = 1.51$ and $E/J \approx 0.05$, and these results place NBCT in the large- D quantum paramagnetic phase but exceedingly close to a long-range ordering transition. These findings are significantly different from the initial interpretations that this system was in the Haldane phase with $D/J \approx 0.88$ [14]. Consequently, NBCT is a prime candidate for pressure- or doping-induced quantum criticality. Moreover, the importance of rhombic anisotropy in regions close to the D_C/J critical points is emphasized by NBCT. Additionally, doping or grinding experiments to look for end-chain spins and confirm or disprove the proposed non-Haldane ground state for NBCT will be useful, as would specific heat measurements down to 0.3 K or less. The synthesis of sizable (> 100 mg) single crystals would also allow for more investigation of NBCT at low temperature and in finite magnetic fields.

The Department of Energy will provide public access to these results of federally sponsored research in accordance with the DOE Public Access Plan [23].

ACKNOWLEDGMENTS

D.M.P. and A.A.P. are supported through the Scientific User Facilities Division of the Department of Energy (DOE) Office of Science, sponsored by the Basic Energy Science (BES) Program, DOE Office of Science. This research used resources at the Spallation Neutron Source, a DOE Office of Science User Facility operated by the Oak Ridge National Laboratory (ORNL). J.H. was supported by the U.S. DOE Office of Science, sponsored by the BES Program in Materials Sciences and Engineering Division of ORNL and by the Polish National Agency of Academic Exchange (NAWA) under Contract No. PPN/PPO/2018/1/00035. Aspects of this work were partially supported by funding provided by the National Science Foundation via Grants No. DMR-1703003 (J.L.M.) and No. DMR-1708410 (M.W.M.). A portion of this work was performed at the National High Magnetic Field Laboratory,

which is supported by National Science Foundation Cooperative Agreement No. DMR-1644779 and the state of Florida. We acknowledge C. Batista, A. Tselik, and G. E. Granroth for conversations about analyzing the data. We acknowledge M. Whangbo for a calculation of the single-ion anisotropy and G. Alvarez for developing the DMRG++ code [24]. This work has been partially supported by U.S. DOE Grant No. DE-FG02-13ER41967. ORNL is managed by UT-Battelle, LLC, under Contract No. DE-AC05-00OR22725 for the U.S. Department of Energy. The U.S. Government retains, and the publisher, by accepting the article for publication, acknowledges that the U.S. Government retains a nonexclusive, paid-up, irrevocable, worldwide license to publish or reproduce the published form of this manuscript or allow others to do so for U.S. Government purposes.

APPENDIX A: TECHNICAL DETAILS

All reactions for NBCT synthesis were carried out using PLASTICWARE. $^{11}\text{B}(\text{OH})_3$ was obtained from Aldrich Chemical, and 3-chloropyridine- D_4 (98.9% atom %D) was purchased from CDN Isotopes. Each was used without purification.

$\text{H } ^{11}\text{BF}_4$. A 4.000-g (64.5-mmol) mass of $^{11}\text{B}(\text{OH})_3$ was dissolved in 6.5 mL of $\text{HF}(\text{aq})$ ($d = 1.16$ g/mL; 258 mmol) while stirring to produce a theoretical yield of 5.676 g of aqueous $\text{H } ^{11}\text{BF}_4$.

$\text{Ni}(^{11}\text{BF}_4)_2 \cdot y\text{H}_2\text{O}$. While stirring, the colorless $\text{H } ^{11}\text{BF}_4$ solution was completely added to 3.828 g of neat NiCO_3 to produce a dark green solution from which $\text{CO}_2(\text{g})$ evolved. The reaction mixture was allowed to stir for about 30 min until cessation of bubbling CO_2 , leaving a clear green solution that was lighter in color. The solution was heated while stirring for approximately 2 h to remove the H_2O solvent, at which point a moist emerald green solid of $\text{Ni}(^{11}\text{BF}_4)_2$ was retrieved.

$[\text{Ni}(\text{HF}_2)(3\text{-Clpyridine-}D_4)_4] ^{11}\text{BF}_4$. $\text{Ni}(^{11}\text{BF}_4)_2 \cdot y\text{H}_2\text{O}$ (0.7917 g, 3.40 mmol) and NH_4HF_2 (0.1939 g, 3.40 mmol) were dissolved together in 4 mL of H_2O to produce a light green solution. This solution was added to neat 3-chloropyridine- D_4 (2.000 g, 17.01 mmol) to yield a turquoise-colored solution. The plastic beaker was covered with perforated Parafilm and allowed to slowly evaporate at room temperature. After 4 days, a large mass of turquoise blue solid had formed which was collected by vacuum filtration to afford 1.4082 g of microcrystalline product. The product identity was established by infrared spectroscopy and single-crystal x-ray diffraction and was shown to be the desired $[\text{Ni}(\text{HF}_2)(3\text{-Clpyridine-}D_4)_4] ^{11}\text{BF}_4$ material. The low-field magnetic response of a small sample (nominally 15 mg) was studied using a commercial superconducting quantum interference device magnetometer (MPMS-XL), and to within experimental uncertainties, the measured temperature dependence ($5 \text{ K} \leq T \leq 300 \text{ K}$) was the same as reported Ref. [14].

For the neutron experiments, ≈ 1 g of powder was mounted in an aluminum can with a copper lid. Cryogenic temperatures were achieved with a wet ^3He cryostat for the $T = 0.3 \text{ K}$ and $T = 13 \text{ K}$ data and a cryogen-free dilution fridge for the $T = 0.07 \text{ K}$ data. The time-of-flight spectrometer at the SNS BL-5 cold chopper neutron spectrometer (CNCS) was used in high-flux mode [25]. Experimental energy resolutions are

from MANTID [26], and at $\hbar\omega = 0$ the full width at half maximum resolution was 0.02 and 0.11 meV for 1- and 3.32-meV incident energies, respectively. The data were normalized to the proton current on target during collection. The detectors were normalized using a vanadium standard measurement that is defined to have an average intensity per pixel of one scaled unit. Intensities are multiplied by the ratio of incident and final momenta to result in numbers that are proportional to a correlation function. All numerical optimizations used the libraries of SCIPY [27].

The DMRG calculations were performed for $D/J = [0, 0.5, 1.0, 1.5, 2.0]$ using $L = 64$ sites on a chain. For $\omega/J < 0.2$, $\Delta\omega/J = 0.002$, and $\eta = 0.0032$. For $\omega/J > 0.2$, $\Delta\omega/J = 0.04$, and $\eta = 0.07$. For denoising, these DMRG correlations were fit to the phenomenological relationships

$$I(q_{1D}, \hbar\omega) = [1 - \cos(q_{1D})] \left(I_0 + \frac{I_{-1}}{\hbar\omega} \right),$$

$$\frac{E(q_{1D})}{J} = \sqrt{A \cos\left(\frac{q_{1D}}{2}\right)^2 + v^2 \sin^2(q_{1D}) + \Delta^2}, \quad (\text{A1})$$

where the dispersion relationship parametrization is inspired by linear spin wave theory [28]. The resulting parameters were then interpolated with cubic splines to give smooth functions of A , v , Δ , I_0 , and I_{-1} for the $\langle S^{x/y} S^{x/y} \rangle$ and $\langle S^z S^z \rangle$ correlation functions. The $\langle S^{x/y} S^{x/y} \rangle$ correlations were further split into $\langle S^x S^x \rangle$ and $\langle S^y S^y \rangle$ by letting $\Delta_{x/y} \rightarrow \Delta_{x/y} \pm \Delta_E/2$. To compare DMRG with experiment, a Bose factor was included to modify the intensity as a function of $\hbar\omega$. The Ni^{2+} magnetic form factor was included to modify the intensity as a function of momentum transfer [29]. Subsequent to fitting with the $D/J = [0, 0.5, 1.0, 1.5, 2.0]$ interpolated DMRG data, a $D/J = 1.51$ DMRG calculation was performed that agreed with the interpolated data to within 1 part per 1000 and therefore had no effect on the solution.

The NBCT and the mononuclear analog $[\text{Ni}(3\text{-Clpyridine})_4(\text{FHF})_2]$ were modeled by wave function theory using a complete active space self-consistent-field approach employing the scalar relativistically recontracted basis sets tailored for use with the Douglas-Kroll-Hess (DKH) Hamiltonian. Calculations were done in the ORCA program suite [30]. The basis sets were of triple- ζ (TZ) quality with valence (V) orbitals and polarization (P) functions (DKH-def2-TZVP) except for Zr, where the ‘‘old-DKH-TZVP’’ of ORCA was employed. In all calculations, the second-order DKH Hamiltonian was used. The calculation was done on the experimental geometry, and the active space was limited to the Ni d orbitals, leading to a complete active space self-consistent field having 8 active electrons and 5 active orbitals (CAS(8,5)) calculation.

APPENDIX B: LOCAL MODE AND EXAMPLE OF $I(Q_{1D})$ EXTRACTION

The local mode we assign to single-ion D excitations from Ni^{2+} spins without spatial correlation is visible in the raw powder data at $T = 0.3 \text{ K}$ [Fig. 5(a)]. At low momentum transfers, the contaminating intensity from the direct beam is visible. Multiple scattering between the sample and the cryostat is also visible, such as at $(|Q|, \hbar\omega) \approx (1^{-1}, 0.6 \text{ meV})$.

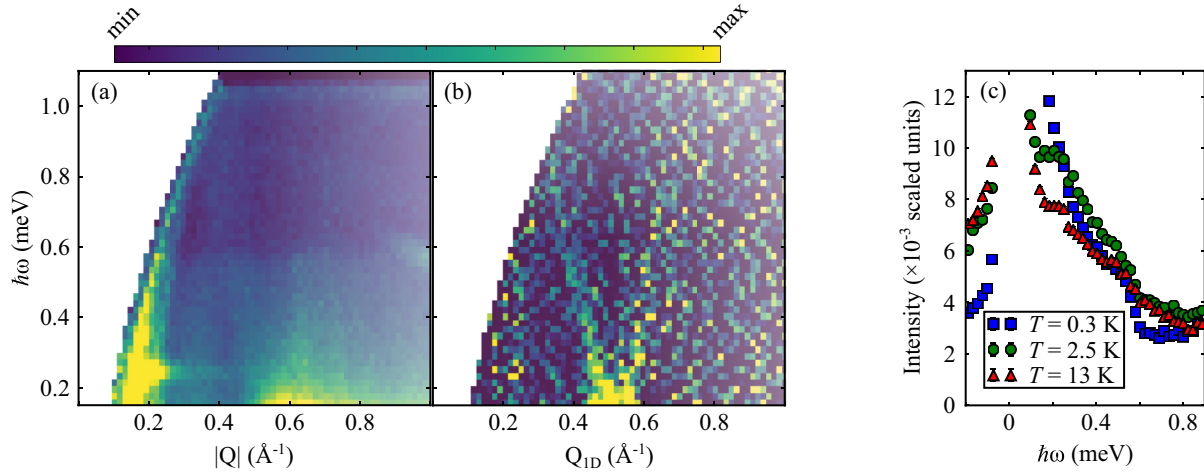


FIG. 5. Local mode in NBCT. (a) $E_i = 1.55$ meV, $T = 0.3$ K data, with min = 0 and max = 2×10^{-2} intensity scale. (b) $E_i = 1.55$ meV, $T = 0.3$ K data minus $T = 13$ K data with min = -1×10^{-5} and max = 1×10^{-4} intensity scale. In (a) and (b), white regions are where the scattering condition is not satisfied by the spectrometer. (c) Intensity versus energy transfer for $E_i = 1.55$ meV powder averaged data near $q_{1D} = \pi$ (Q_{1D} averaged between $[0.4, 0.6]^{-1}$).

Here, we also visualize the extraction of the one-dimensional correlations from the powder averaged data. Subtracting $T = 13$ K data from $T = 0.3$ K data removes extrinsic features, and subsequently, converting from $|Q|$ to Q_{1D} removes the

bleeding of intensity to higher momenta [Fig. 5(b)]. The temperature dependence of the raw powder data averaged over $|Q| = [0.4, 0.6]^{-1}$ shows the evolution of both the one-dimensional collective modes and the local mode [Fig. 5(c)].

- [1] I. Affleck, Quantum spin chains and the Haldane gap, *J. Phys.: Condens. Matter* **1**, 3047 (1989).
- [2] H. Bethe, Zur Theorie der Metalle, *Z. Phys.* **71**, 205 (1931).
- [3] F. D. M. Haldane, Nonlinear Field Theory of Large-Spin Heisenberg Antiferromagnets: Semiclassically Quantized Solitons of the One-Dimensional Easy-Axis Néel State, *Phys. Rev. Lett.* **50**, 1153 (1983).
- [4] F. Haldane, Continuum dynamics of the 1-D Heisenberg antiferromagnet: Identification with the O(3) nonlinear sigma model, *Phys. Lett. A* **93**, 464 (1983).
- [5] F. D. M. Haldane, Nobel Lecture: Topological quantum matter, *Rev. Mod. Phys.* **89**, 040502 (2017).
- [6] X.-G. Wen, Colloquium: Zoo of quantum-topological phases of matter, *Rev. Mod. Phys.* **89**, 041004 (2017).
- [7] M. den Nijs and K. Rommelse, Preroughening transitions in crystal surfaces and valence-bond phases in quantum spin chains, *Phys. Rev. B* **40**, 4709 (1989).
- [8] S. Hu, B. Normand, X. Wang, and L. Yu, Accurate determination of the Gaussian transition in spin-1 chains with single-ion anisotropy, *Phys. Rev. B* **84**, 220402(R) (2011).
- [9] W. Chen, K. Hida, and B. C. Sanctuary, Ground-state phase diagram of $S = 1$ XXZ chains with uniaxial single-ion-type anisotropy, *Phys. Rev. B* **67**, 104401 (2003).
- [10] Y.-C. Tzeng, H. Onishi, T. Okubo, and Y.-J. Kao, Quantum phase transitions driven by rhombic-type single-ion anisotropy in the $S = 1$ Haldane chain, *Phys. Rev. B* **96**, 060404(R) (2017).
- [11] A. F. Albuquerque, C. J. Hamer, and J. Oitmaa, Quantum phase diagram and excitations for the one-dimensional $S = 1$ Heisenberg antiferromagnet with single-ion anisotropy, *Phys. Rev. B* **79**, 054412 (2009).
- [12] S. R. White and D. A. Huse, Numerical renormalization-group study of low-lying eigenstates of the antiferromagnetic $S = 1$ Heisenberg chain, *Phys. Rev. B* **48**, 3844 (1993).
- [13] K. Wierschem and P. Sengupta, Characterizing the Haldane phase in quasi-one-dimensional spin-1 Heisenberg antiferromagnets, *Mod. Phys. Lett. B* **28**, 1430017 (2014).
- [14] J. L. Manson, A. G. Baldwin, B. L. Scott, J. Bendix, R. E. D. Sesto, P. A. Goddard, Y. Kohama, H. E. Tran, S. Ghannadzadeh, J. Singleton, T. Lancaster, J. S. Möller, S. J. Blundell, F. L. Pratt, V. S. Zapf, J. Kang, C. Lee, M. H. Whangbo, and C. Baines, $[\text{Ni}(\text{HF}_2)(3 - \text{Clpy})_4]\text{BF}_4$ (py = pyridine): Evidence for spin exchange along strongly distorted F – H – F⁻ bridges in a one-dimensional polymeric chain, *Inorg. Chem.* **51**, 7520 (2012).
- [15] J.-S. Xia, A. Ozarowski, P. M. Spurgeon, A. G. Graham, J. L. Manson, and M. W. Meisel, Unusual magnetic response of an $S = 1$ antiferromagnetic linear-chain material, *J. Phys.: Conf. Ser.* **969**, 012121 (2018).
- [16] U. Schollwöck, The density-matrix renormalization group, *Rev. Mod. Phys.* **77**, 259 (2005).
- [17] C. Broholm, G. Aeppli, Y. Chen, D. C. Dender, M. Enderle, P. R. Hammar, Z. Honda, K. Katsumata, C. P. Landee, M. Oshikawa, L. P. Regnault, D. H. Reich, S. M. Shapiro, M. Sieling, M. B. Stone, M. M. Turnbull, I. Zaliznyak, and A. Zheludev, Magnetized States of Quantum Spin Chains, in *High Magnetic Fields: Applications in Condensed Matter Physics and Spectroscopy*, edited by C. Berthier, L. P. Lévy, and G. Martinez (Springer, Berlin, 2001), pp. 211–234.
- [18] K. Tomiyasu, M. Fujita, A. I. Kolesnikov, R. I. Bewley, M. J. Bull, and S. M. Bennington, Conversion method of powder

- inelastic scattering data for one-dimensional systems, *Appl. Phys. Lett.* **94**, 092502 (2009).
- [19] J. L. Manson, Z. E. Manson, A. Sargent, D. Y. Villa, N. L. Etten, W. J. A. Blackmore, S. P. M. Curley, R. C. Williams, J. Brambleby, P. A. Goddard, A. Ozarowski, M. N. Wilson, B. M. Huddart, T. Lancaster, R. D. Johnson, S. J. Blundell, J. Bendix, K. A. Wheeler, S. H. Lapidus, F. Xiao, S. Birnbaum, and J. Singleton, Enhancing easy-plane anisotropy in bespoke Ni(II) quantum magnets, *Polyhedron* **180**, 114379 (2020).
- [20] L. P. Regnault, I. Zaliznyak, J. P. Renard, and C. Vettier, Inelastic-neutron-scattering study of the spin dynamics in the Haldane-gap system $\text{Ni}(\text{C}_2\text{H}_8\text{N}_2)_2\text{NO}_2\text{ClO}_4$, *Phys. Rev. B* **50**, 9174 (1994).
- [21] C. Rudowicz, Effect of small in-plane anisotropy in the large-D phase systems based on Ni^{2+} ($S=1$) ions in Heisenberg antiferromagnetic chains, *Physica B (Amsterdam, Neth.)* **436**, 193 (2014).
- [22] O. Golinelli, T. Jolicoeur, and R. Lacaze, Dispersion of magnetic excitations in a spin-1 chain with easy-plane anisotropy, *Phys. Rev. B* **46**, 10854 (1992).
- [23] <http://energy.gov/downloads/doe-public-access-plan>.
- [24] DMRG++, <https://g1257.github.io/dmrgPlusPlus/>.
- [25] G. Ehlers, A. Podlesnyak, J. L. Niedziela, E. B. Iverson, and P. E. Sokol, The new cold neutron chopper spectrometer at the spallation neutron source: Design and performance, *Rev. Sci. Instrum.* **82**, 085108 (2011).
- [26] O. Arnold, J. C. Bilheux, J. M. Borreguero, A. Buts, S. I. Campbell, L. Chapon, M. Doucet, N. Draper, R. F. Leal, M. A. Gigg, V. E. Lynch, A. Markvardsen, D. J. Mikkelsen, R. L. Mikkelsen, R. Miller, K. Palmén, P. Parker, G. Passos, T. G. Perring, P. F. Peterson, S. Ren, M. A. Reuter, A. T. Savici, J. W. Taylor, R. J. Taylor, R. Tolchenov, W. Zhou, and J. Zikovsky, Mantid – Data analysis and visualization package for neutron scattering and μSR experiments, *Nucl. Instrum. Methods Phys. Res., Sect. A* **764**, 156 (2014).
- [27] P. Virtanen, R. Gommers, T. E. Oliphant, M. Haberland, T. Reddy, D. Cournapeau, E. Burovski, P. Peterson, W. Weckesser, J. Bright *et al.*, *Nat. Methods* **17**, 261 (2020).
- [28] S. Ma, C. Broholm, D. H. Reich, B. J. Sternlieb, and R. W. Erwin, Dominance of Long-Lived Excitations in the Antiferromagnetic Spin-1 Chain NENP, *Phys. Rev. Lett.* **69**, 3571 (1992).
- [29] H. Börner, J. Brown, C. J. Carlile, R. Cubitt, R. Currat, A. J. Dianoux, B. Farago, A. W. Hewat, J. Kulda, E. Lelièvre-Berna, G. J. McIntyre, S. A. Mason, R. P. May, A. Oed, J. R. Stewart, F. Tasset, J. Tribolet, I. Anderson, and D. W. Dubbers, *Neutron Data Booklet* (Old City Publishing, Philadelphia, 2003).
- [30] F. Neese, The ORCA program system, *Wiley Interdiscip. Rev.: Comput. Mol. Sci.* **2**, 73 (2012).